Available online at www.sciencedirect.com
ScienceDirect
Applied Numerical Mathematics 57 (2007) 697–709
APPLIED NUMERICAL MATHEMATICS
www.elsevier.com/locate/apnum

Dynamics of the center of mass in rotating Bose–Einstein condensates

Yanzhi Zhang, Weizhu Bao *

Department of Mathematics, National University of Singapore, Singapore 117543, Singapore

Available online 23 August 2006

Abstract

In this paper, we derive the analytical solution for a second-order ordinary differential system which governs the motion of the center of mass in the dynamics of a stationary state with its center shifted. A leap-frog Fourier pseudospectral (LFFP) method is presented for efficient and accurate numerical simulations of the Gross–Pitaevskii equation (GPE) with an angular momentum rotation term. Different motion patterns for the center of mass are observed and classified from the analytical solution and confirmed by directly simulating the GPE. To show the effectiveness of the LFFP method, the dynamics of vortex lattices are studied, and the numerical results demonstrate the efficiency and extremely high resolution of our method.

Keywords: Rotating Bose–Einstein condensate; Gross–Pitaevkii equation; Stationary state; Angular momentum rotation; Center of mass; Quantized vortex lattice

1. Introduction

Since the realization of Bose–Einstein condensation (BEC) in dilute bosonic atomic gases [2], much attention has been focused on its dynamical phenomena associated with superfluidity. One remarkable feature of a superfluid is the appearance of quantized vortices. Recently, several groups have observed quantized vortices in rotating BEC [11,10], by imposing a rotating laser beam on the magnetic trap to create an anisotropic rotating harmonic potential.

We consider the dimensionless Gross–Pitaevskii equation (GPE) in d-dimensions ($d = 2, 3$) [6,3]:

$$i\partial_t \psi(\mathbf{x}, t) = -\frac{1}{2}\nabla^2\psi + V_d(\mathbf{x})\psi + \beta_d|\psi|^2\psi - \Omega L_z\psi, \quad \mathbf{x} \in \mathbb{R}^d,\ t > 0, \tag{1.1}$$

$$\psi(\mathbf{x}, 0) = \psi_0(\mathbf{x}), \quad \mathbf{x} \in \mathbb{R}^d, \quad \text{with } \|\psi_0\|^2 := \int_{\mathbb{R}^d} \left|\psi_0(\mathbf{x})\right|^2 d\mathbf{x} = 1, \tag{1.2}$$

where $\psi(\mathbf{x}, t)$ is the macroscopic wave function, $L_z = -i(x\partial_y - y\partial_x)$ is the z-component of the angular momentum, Ω is the angular speed of the laser beam, β_d is a constant characterizing the particle interactions and the external

* Corresponding author. Fax: +65 67746756.
E-mail addresses: zhyanzhi@cz3.nus.edu.sg (Y. Zhang), bao@cz3.nus.edu.sg (W. Bao).
URL: http://www.cz3.nus.edu.sg/~bao/.

0168-9274/$30.00
doi:10.1016/j.apnum.2006.07.011

harmonic oscillator potential $V_d(\mathbf{x}) = (\gamma_x^2 x^2 + \gamma_y^2 y^2)/2$ in two dimensions (2D), and resp. in 3D $V_d(\mathbf{x}) = (\gamma_x^2 x^2 + \gamma_y^2 y^2 + \gamma_z^2 z^2)/2$ with $\gamma_x > 0$, $\gamma_y > 0$ and $\gamma_z > 0$ constants.

The main aim of this paper is: (i) to derive the analytical solution for the second-order ODE system which governs the motion of the center of mass in the dynamics of a stationary state with its center shifted, (ii) to identify typical motion patterns for the center of mass based on different trapping frequencies and angular momentum rotation speed, and (iii) to propose an efficient method for simulating the dynamics of rotating BEC and apply it to verify different motion patterns. In fact, in order to study effectively the dynamics of BEC, especially in the strong repulsive interaction regime, i.e. $\beta_d \gg 1$ in (1.1), an efficient and accurate numerical method is one of the key issues. For non-rotating BEC, i.e. $\Omega = 0$ in (1.1), there have been many numerical methods reported in the literature [4,7,5,12,8]. While for rotating BEC, the available numerical methods are very limited [12,8,3], and most of them have low-order accuracy in space. Recently, Bao et al. [3] proposed an efficient and accurate time-splitting type method, in which the polar coordinate or cylindrical coordinate is adopted so as to make the coefficient of the angular momentum rotation term a constant. In this paper, we try the leap-frog Fourier pseudospectral (LFFP) method in which the Cartesian coordinate is adopted. Both methods are time reversible just as the GPE (1.1) does. Of course, each one has its own advantages and disadvantages. The former is unconditionally stable, implicit in 1D and conserves the total density. It is of spectral accuracy in transverse direction and usually second or fourth-order accuracy in radial direction. The latter is explicit, of spectral accuracy in all directions and easy to program. It is stable under a stability condition. Due to its fully spectral resolution in space, the LFFP method may resolve better the dynamics of vortex lattices in rotating BEC, especially in the regime with strong repulsive interaction, i.e. $\beta_d \gg 1$, and large angular momentum rotation speed, i.e. $|\Omega| \approx \min\{\gamma_x, \gamma_y\}$, where a large number of vortices appear in the condensate and thus spatial resolution is one of the key issues.

The paper is organized as follows. In Section 2, we review the second-order ODE system for the motion of the center of mass, and solve it analytically. In Section 3, we propose the leap-frog Fourier pseudospectral (LFFP) method. Finally, some conclusions are drawn in Section 4.

2. Analytical solutions for the center of mass

Without loss of generality, in this section, we assume $\gamma_x = 1$ and $\gamma_x \leqslant \gamma_y$. Let $\phi_e(\mathbf{x})$ be a stationary state solution of the GPE (1.1) with a chemical potential μ_e, i.e. (μ_e, ϕ_e) satisfying

$$\mu_e \phi_e(\mathbf{x}) = -\frac{1}{2}\nabla^2 \phi_e + V_d(\mathbf{x})\phi_e + \beta_d |\phi_e|^2 \phi_e - \Omega L_z \phi_e, \quad \text{with } \|\phi_e\|^2 = 1. \tag{2.1}$$

If the initial data $\psi_0(\mathbf{x})$ in (1.2) is chosen as a stationary state with its center shifted, i.e.

$$\psi_0(\mathbf{x}) = \phi_e(\mathbf{x} - \mathbf{x}_0), \quad \mathbf{x} \in \mathbb{R}^d, \tag{2.2}$$

where $\mathbf{x}_0$ is a given point in $\mathbb{R}^d$, one can construct an exact solution of the GPE (1.1) with a harmonic oscillator potential [9,7,3],

$$\psi(\mathbf{x}, t) = \phi_e\big(\mathbf{x} - \mathbf{x}(t)\big) e^{-i\mu_e t} e^{iw(\mathbf{x},t)}, \quad \mathbf{x} \in \mathbb{R}^d,\ t \geqslant 0, \tag{2.3}$$

where $w(\mathbf{x}, t)$ is a linear function of $\mathbf{x}$ and $\mathbf{x}(t)$ satisfies the following second-order ODE system [3]:

$$\ddot{x}(t) - 2\Omega \dot{y}(t) + \big(\gamma_x^2 - \Omega^2\big)x(t) = 0, \tag{2.4}$$

$$\ddot{y}(t) + 2\Omega \dot{x}(t) + \big(\gamma_y^2 - \Omega^2\big)y(t) = 0, \quad t \geqslant 0, \tag{2.5}$$

$$x(0) = x_0, \qquad y(0) = y_0, \qquad \dot{x}(0) = \Omega y_0, \qquad \dot{y}(0) = -\Omega x_0, \tag{2.6}$$

in 2D; if in 3D, another ODE needs to be added:

$$\ddot{z}(t) + \gamma_z^2 z(t) = 0, \qquad z(0) = z_0, \qquad \dot{z}(0) = 0. \tag{2.7}$$

This kind of exact solution (2.3) can be used, in particular, in the benchmark and validation of numerical algorithms for the time-dependent GPE. It has been studied in the literature for non-rotating BEC [9,7] and rotating BEC [3]. The physical interpretation of the solution is that it is a soliton-type solution in high dimensions. The experimental realization for the solution is to shift the magnetic trapping center from the origin to the position $-\mathbf{x}_0$, i.e. $V_d(\mathbf{x}) \to V_d(\mathbf{x} + \mathbf{x}_0)$.

From (2.1), (2.3) and changing of variables, we get

$$\langle \mathbf{x} \rangle(t) := \int_{\mathbb{R}^d} \mathbf{x} \big|\psi(\mathbf{x},t)\big|^2 \,\mathrm{d}\mathbf{x} = \int_{\mathbb{R}^d} \mathbf{x} \big|\phi_e\big(\mathbf{x}-\mathbf{x}(t)\big)\big|^2 \,\mathrm{d}\mathbf{x} = \int_{\mathbb{R}^d} \big(\mathbf{x}+\mathbf{x}(t)\big)\big|\phi_e(\mathbf{x})\big|^2 \,\mathrm{d}\mathbf{x} = \mathbf{x}(t), \quad t \geqslant 0. \tag{2.8}$$

This implies that the dynamics of the center of mass is the same as that of $\mathbf{x}(t)$, i.e. satisfying the ODE system (2.4)–(2.7). It is easy to see that the solution of (2.7) is

$$z(t) = z_0 \cos(\gamma_z t), \quad t \geqslant 0, \tag{2.9}$$

and thus $z(t)$ is a periodic function with period $T_z = 2\pi/\gamma_z$. Furthermore, when $\Omega \neq 0$, we can divide both sides of (2.4) by 2Ω to get

$$\dot{y}(t) = \frac{1}{2\Omega}\big(\ddot{x}(t) + \big(\gamma_x^2 - \Omega^2\big)x(t)\big), \quad t \geqslant 0. \tag{2.10}$$

On the other hand, differentiating (2.5) with respect to t, we obtain

$$y^{(3)}(t) + 2\Omega\ddot{x}(t) + \big(\gamma_y^2 - \Omega^2\big)\dot{y}(t) = 0, \quad t \geqslant 0. \tag{2.11}$$

Plugging (2.10) into (2.11), we get the following fourth-order ODE for $x(t)$,

$$x^{(4)}(t) + \big(\gamma_x^2 + \gamma_y^2 + 2\Omega^2\big)\ddot{x}(t) + \big(\gamma_x^2 - \Omega^2\big)\big(\gamma_y^2 - \Omega^2\big)x(t) = 0, \quad t \geqslant 0. \tag{2.12}$$

The characteristic equation of (2.12) is

$$\lambda^4 + \big(\gamma_x^2 + \gamma_y^2 + 2\Omega^2\big)\lambda^2 + \big(\gamma_x^2 - \Omega^2\big)\big(\gamma_y^2 - \Omega^2\big) = 0. \tag{2.13}$$

In the following subsections, we discuss the solutions of the ODE system (2.4)–(2.6) in different parameter regimes of trapping frequencies and angular rotation speed Ω.

2.1. In a non-rotating BEC

For a non-rotating BEC, i.e. $\Omega = 0$ in (1.1), the second-order ODE system (2.4)–(2.6) collapses to

$$\ddot{x}(t) + \gamma_x^2 x(t) = 0, \qquad \ddot{y}(t) + \gamma_y^2 y(t) = 0, \quad t \geqslant 0, \tag{2.14}$$

$$x(0) = x_0, \qquad y(0) = y_0, \qquad \dot{x}(0) = \dot{y}(0) = 0. \tag{2.15}$$

It is straightforward to see that the solution of (2.14), (2.15) is

$$x(t) = x_0 \cos(\gamma_x t), \qquad y(t) = y_0 \cos(\gamma_y t), \quad t \geqslant 0, \tag{2.16}$$

which implies that both $x(t)$ and $y(t)$ are periodic functions with periods $T_x = 2\pi/\gamma_x$ and $T_y = 2\pi/\gamma_y$, respectively.

Fig. 1 displays the time evolution of the center $\mathbf{x}(t)$ in 2D with $\mathbf{x}_0 = (1,1)^T$ for different γ_x and γ_y, and Fig. 2 shows similar results in 3D with $\mathbf{x}_0 = (1,1,1)^T$. From Figs. 1 and 2, we can draw the following conclusions for the motion of the center $\mathbf{x}(t)$ in non-rotating BEC: (i) Each component of the center $\mathbf{x}(t)$ is a periodic function with the same frequency as the trapping frequency in that direction (cf. Fig. 1). (ii) In 2D with a radially symmetric trap or 3D with a spherically symmetric trap, the center moves like a pendulum with period $T = 2\pi/\gamma_x$, and its trajectory is a straight segment (cf. Figs. 1(a) and 2(a)). (iii) In 2D, if γ_y/γ_x is a rational number, i.e. $\gamma_y/\gamma_x = q/p$ with q and p positive integers and no common factor, then the center moves periodically with period $2p\pi$ (cf. Fig. 1(b)). On the other hand, if γ_y/γ_x is an irrational number, the center moves chaotically in the rectangle $\Omega_{\mathbf{x}} = [-|x_0|, |x_0|] \times [-|y_0|, |y_0|]$, and the envelope of its trajectory is the boundary of the rectangle $\Omega_{\mathbf{x}}$ (cf. Fig. 1(c)). (iv) In 3D, if both γ_y/γ_x and γ_z/γ_x are rational numbers, the center moves periodically (cf. Fig. 2(b)); if both of them are irrational numbers, the center moves in a 3D box (cf. Fig. 2(d)); otherwise, it moves in a 2D rectangle (cf. Fig. 2(c)).

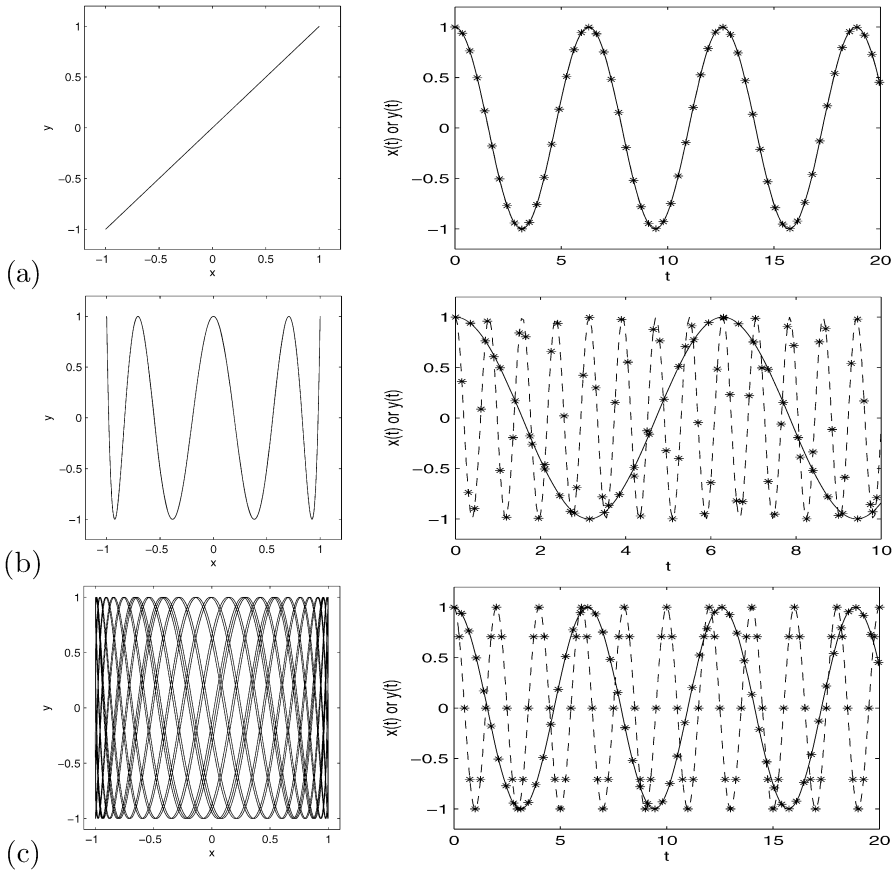

Fig. 1. Motion of the center $\mathbf{x}(t)$ in 2D for a non-rotating BEC. Left: trajectory $\mathbf{x}(t)$ for $t \in [0, 50]$; Right: time evolution of $x(t)$ (solid line) and $y(t)$ (dash line), where '$*$' is obtained by directly simulating the GPE (1.1). (a) $\gamma_x = \gamma_y = 1$; (b) $\gamma_x = 1$, $\gamma_y = 8$; (c) $\gamma_x = 1$, $\gamma_y = 2\pi$.

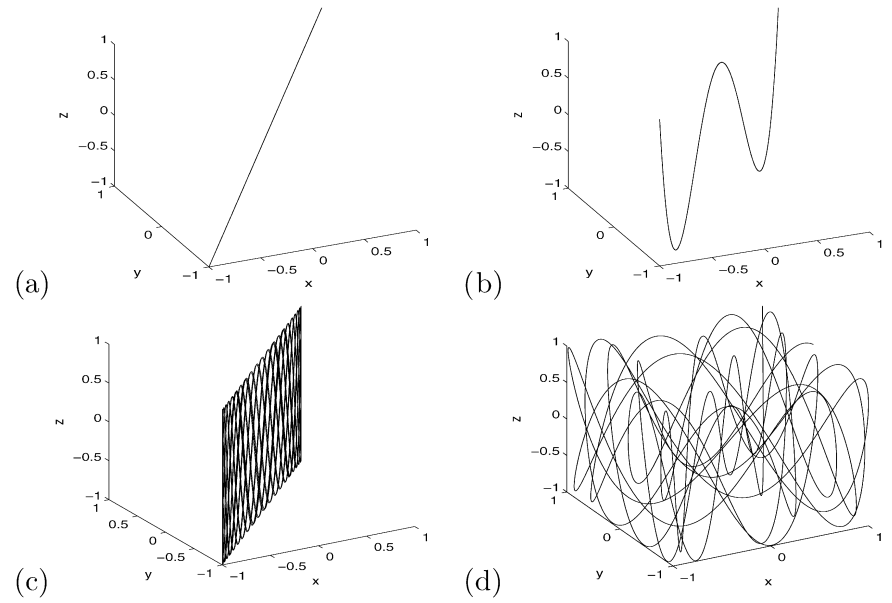

Fig. 2. Trajectory of the center $\mathbf{x}(t)$ in 3D for a non-rotating BEC. (a) $\gamma_x = \gamma_y = \gamma_z = 1$; (b) $\gamma_x = \gamma_y = 1$, $\gamma_z = 4$; (c) $\gamma_x = \gamma_y = 1$, $\gamma_z = 2\pi$; (d) $\gamma_x = 1$, $\gamma_y = \sqrt{2}$, $\gamma_z = \pi$.

2.2. In a rotating BEC with an isotropic potential

For a rotating BEC with an isotropic potential, i.e. $\Omega \neq 0$ and $\gamma_x = \gamma_y$, we have the following solutions for the second-order ODE system (2.4)–(2.6):

Lemma 2.1. *If $\Omega \neq 0$ and $\gamma_x = \gamma_y$ in* (2.4)–(2.6)*, the solutions $x(t)$ and $y(t)$ for the motion of the center are*

$$x(t) = \frac{x_0}{2}\big[\cos(at) + \cos(bt)\big] + \frac{|\Omega| y_0}{2\Omega}\big[\sin(at) - \sin(bt)\big], \tag{2.17}$$

$$y(t) = \frac{y_0}{2}\big[\cos(at) + \cos(bt)\big] + \frac{|\Omega| x_0}{2\Omega}\big[-\sin(at) + \sin(bt)\big], \quad t \geqslant 0, \tag{2.18}$$

where $a = \gamma_x + |\Omega|$ and $b = \gamma_x - |\Omega|$. Furthermore, we can get the distance between the center of mass and the trap center is a periodic function with period $T = \pi/\gamma_x$, i.e.

$$\big|\mathbf{x}(t)\big| := \sqrt{x^2(t) + y^2(t)} = \sqrt{x_0^2 + y_0^2}\,\big|\cos(\gamma_x t)\big|, \quad t \geqslant 0. \tag{2.19}$$

Proof. When $\gamma_x = \gamma_y$, the characteristic Eq. (2.13) becomes

$$\lambda^4 + 2\big(\gamma_x^2 + \Omega^2\big)\lambda^2 + \big(\gamma_x^2 - \Omega^2\big)^2 = 0. \tag{2.20}$$

Solving (2.20), we get its roots as

$$\lambda_{1,2} = \pm i\big(\gamma_x + |\Omega|\big) = \pm ai, \qquad \lambda_{3,4} = \pm i\big(\gamma_x - |\Omega|\big) = \pm bi. \tag{2.21}$$

Thus the general solution of the ODE (2.12) is

$$x(t) = c_1\cos(at) + c_2\sin(at) + c_3\cos(bt) + c_4\sin(bt), \quad t \geqslant 0, \tag{2.22}$$

where c_1, c_2, c_3 and c_4 are constants. Plugging (2.22) into (2.10) and then integrating with respect to t, we get the general solution for $y(t)$,

$$y(t) = -\frac{|\Omega|}{\Omega}\big[c_1\sin(at) - c_2\cos(at)\big] + \frac{|\Omega|}{\Omega}\big[c_3\sin(bt) - c_4\cos(bt)\big] + c_5, \quad t \geqslant 0. \tag{2.23}$$

Taking $t = 0$ in (2.22) and (2.23), and noticing (2.4) and (2.6), we have

$$c_5 = 0, \qquad c_1 + c_3 = x_0, \qquad ac_2 + bc_4 = \Omega y_0, \qquad \frac{|\Omega|}{\Omega}(c_2 - c_4) = y_0, \qquad \frac{|\Omega|}{\Omega}(bc_3 - ac_1) = -\Omega x_0.$$

Solving the above equations, we get

$$c_1 = c_3 = \frac{x_0}{2}, \qquad c_2 = -c_4 = \frac{\Omega y_0}{2|\Omega|}, \qquad c_5 = 0. \tag{2.24}$$

Thus the solution (2.17), (2.18) is a combination of (2.22), (2.23) and (2.24). Furthermore, from (2.17), (2.18), we can obtain

$$\begin{aligned}
\big|\mathbf{x}(t)\big|^2 &= x(t)^2 + y(t)^2 \\
&= \left[\frac{x_0}{2}\big(\cos(at) + \cos(bt)\big) + \frac{|\Omega| y_0}{2\Omega}\big(\sin(at) - \sin(bt)\big)\right]^2 \\
&\quad + \left[\frac{y_0}{2}\big(\cos(at) + \cos(bt)\big) + \frac{|\Omega| x_0}{2\Omega}\big(-\sin(at) + \sin(bt)\big)\right]^2 \\
&= \frac{x_0^2}{4}\big[2 + 2\cos\big((a+b)t\big)\big] + \frac{y_0^2}{4}\big[2 + 2\cos\big((a+b)t\big)\big] = \big(x_0^2 + y_0^2\big)\cos^2(\gamma_x t), \quad t \geqslant 0,
\end{aligned} \tag{2.25}$$

which gives (2.19) immediately. □

Fig. 3 shows the time evolutions of the center $\mathbf{x}(t)$ with $\gamma_x = \gamma_y = 1$ and $\mathbf{x}_0 = (1, 1)^T$ for different Ω. Fig. 4 depicts the distance between the center of mass and trap center, i.e. $|\mathbf{x}(t)|$, for different Ω. From Figs. 3 and 4, we can draw

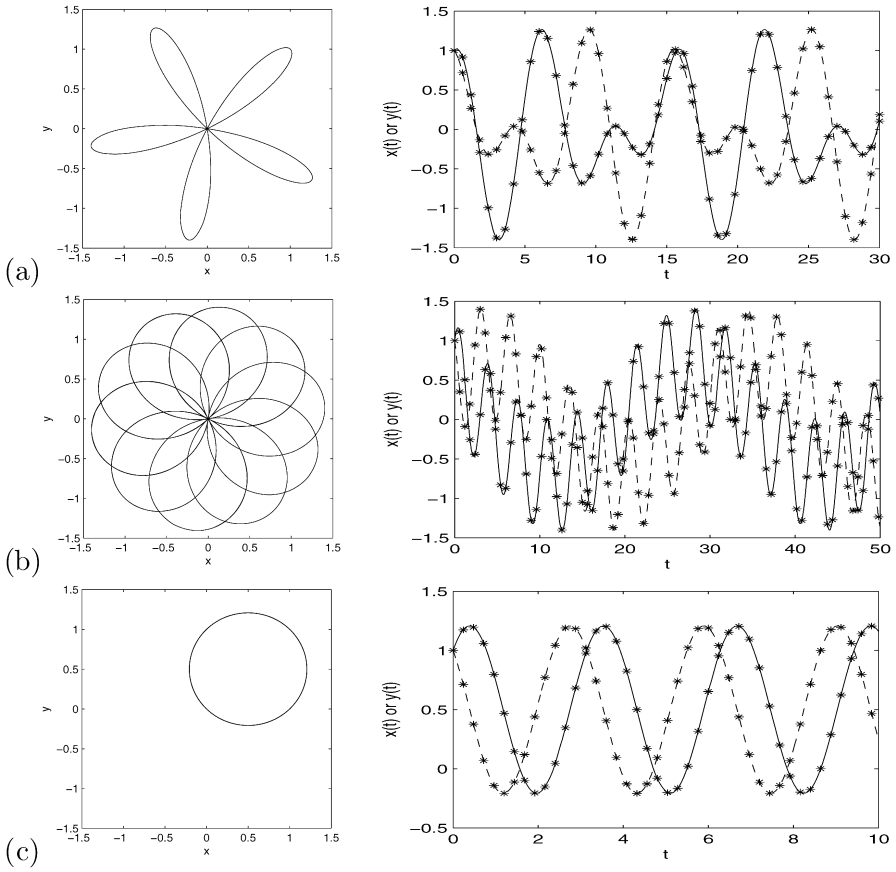

Fig. 3. Motion of the center $\mathbf{x}(t)$ in 2D for a rotating BEC. Left: trajectory $\mathbf{x}(t)$ for $t \in [0, 100]$; Right: time evolution of $x(t)$ (solid line) and $y(t)$ (dash line), where '$*$' is obtained by directly simulating the GPE (1.1). (a) $\Omega = 1/5$; (b) $\Omega = 4/5$; (c) $\Omega = 1$; (d) $\Omega = 3/2$; (e) $\Omega = 6$; (f) $\Omega = \pi$.

the following conclusions for the motion of the center $\mathbf{x}(t)$ in rotating BEC with an isotropic potential: (i) For any angular rotation speed Ω, the distance between the center of mass and the trap center is a periodic function with a period $T = \pi/\gamma_x$ (cf. Fig. 4). (ii) When Ω is a rational number, i.e. $|\Omega| = q/p$ with q and p positive integers and no common factor, the center moves periodically with a period $T = p\pi$ if both q and p are odd integers (cf. Fig. 3(a) and (c)); otherwise $T = 2p\pi$ (cf. Fig. 3(b), (d) and (e)). Furthermore, the graph of its trajectory is unchanged under a rotation of the angle $\theta = 2m\pi\omega$ with m an integer and $\omega = 2\pi/T$ the angular frequency of the motion (cf. Fig. 3(a)–(e)). (iii) When Ω is an irrational number, the center moves chaotically (cf. Fig. 3(f)), but the envelope of its trajectory is a circle centered at the origin with the radius $r = |\mathbf{x}_0|$ (cf. Fig. 3(f)).

2.3. In a rotating BEC with an anisotropic potential

For a rotating BEC with an anisotropic potential, i.e. $\Omega \neq 0$ and $\gamma_x \neq \gamma_y$, we present the analytical solutions of (2.4)–(2.6) in four different cases: (a) $|\Omega| = \gamma_x$; (b) $|\Omega| = \gamma_y$; (c) $0 < |\Omega| < \gamma_x$ or $|\Omega| > \gamma_y$; (d) $\gamma_x < |\Omega| < \gamma_y$. For $|\Omega| = \gamma_x < \gamma_y$, we have

Lemma 2.2. *If $|\Omega| = \gamma_x < \gamma_y$ in* (2.4)–(2.6)*, the solutions $x(t)$ and $y(t)$ for the motion of the center are*

$$x(t) = \frac{x_0}{a^2}\left[\left(\gamma_y^2 + \Omega^2\right) + 2\Omega^2\cos(at)\right] + \frac{\Omega y_0}{a^2}\left[-\left(\gamma_y^2 - \Omega^2\right)t + \frac{2(\gamma_y^2 + \Omega^2)}{a}\sin(at)\right], \tag{2.26}$$

$$y(t) = \frac{y_0}{a^2}\left[2\Omega^2 + \left(\gamma_y^2 + \Omega^2\right)\cos(at)\right] - \frac{\Omega x_0}{a}\sin(at), \quad t \geqslant 0; \tag{2.27}$$

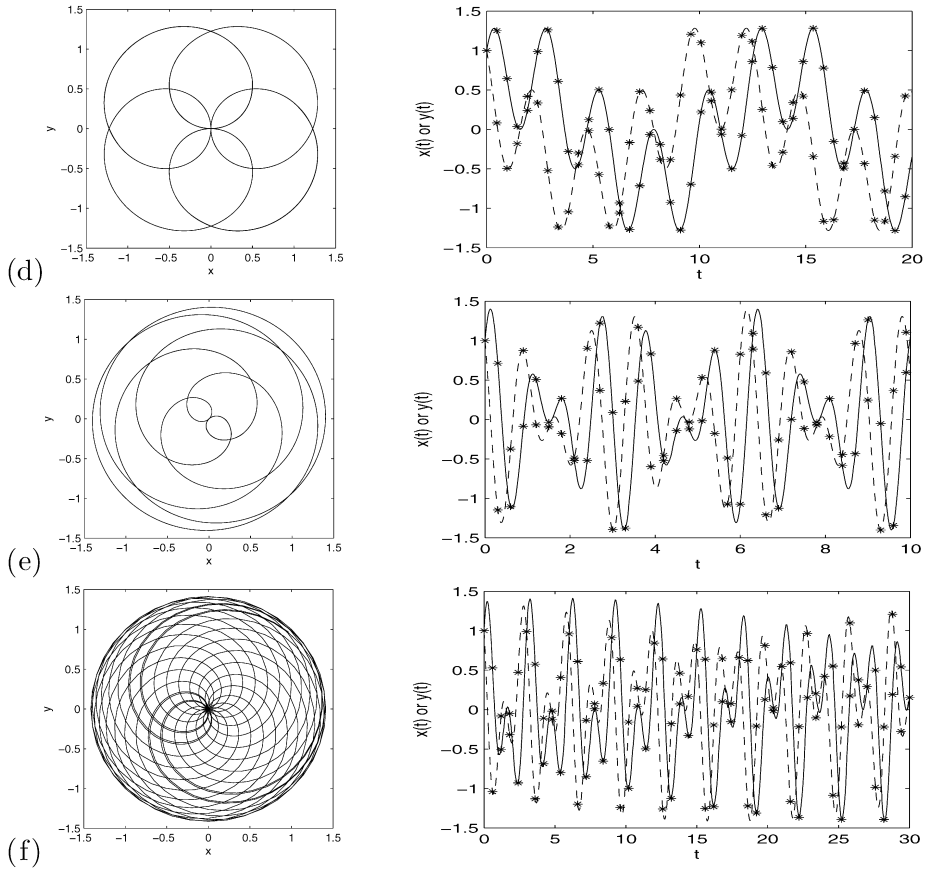

Fig. 3. (*continued*)

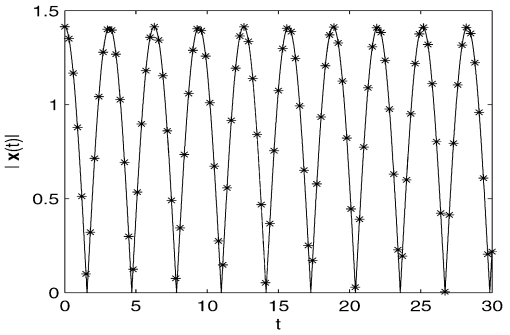

Fig. 4. Distance between the center of mass and the trap center, i.e. $|\mathbf{x}(t)|$, for different Ω, where '$*$' is obtained by directly simulating the GPE (1.1).

where $a = \sqrt{\gamma_y^2 + 3\Omega^2}$. *This implies that the center moves on an ellipse when* $y_0 = 0$, *and moves to infinity when* $y_0 \neq 0$.

Proof. When $|\Omega| = \gamma_x < \gamma_y$, the ODE system (2.4), (2.5) collapses to

$$\ddot{x}(t) - 2\Omega\dot{y}(t) = 0, \tag{2.28}$$

$$\ddot{y}(t) + 2\Omega\dot{x}(t) + \left(\gamma_y^2 - \Omega^2\right)y(t) = 0, \quad t > 0. \tag{2.29}$$

Differentiating (2.29) with respect to t and noticing (2.28), we obtain

$$y^{(3)}(t) + \left(\gamma_y^2 + 3\Omega^2\right)\dot{y}(t) = 0, \quad t \geqslant 0. \tag{2.30}$$

The characteristic equation of (2.30) is

$$\lambda^3 + \left(\gamma_y^2 + 3\Omega^2\right)\lambda = 0. \tag{2.31}$$

Solving (2.31), we obtain

$$\lambda_1 = 0, \qquad \lambda_{2,3} = \pm i\sqrt{\gamma_y^2 + 3\Omega^2} = \pm ai, \tag{2.32}$$

which imply that the general solution of the ODE (2.30) has the form

$$y(t) = c_1 + c_2\cos(at) + c_3\sin(at), \tag{2.33}$$

where c_1, c_2 and c_3 are constants. Plugging (2.33) into (2.28) and integrating with respect to t, we obtain the general solution for $x(t)$ as

$$x(t) = -\frac{(\gamma_y^2 - \Omega^2)c_1}{2\Omega}t + \frac{2\Omega}{a}\left[c_2\sin(at) - c_3\cos(at)\right] + c_4 \tag{2.34}$$

with c_4 a constant. Taking $t = 0$ in (2.33) and (2.34), and noticing (2.6), we have

$$c_4 - \frac{2\Omega}{a}c_3 = x_0, \qquad 2\Omega c_2 - \frac{\gamma_y^2 - \Omega^2}{2\Omega}c_1 = \Omega y_0, \qquad c_1 + c_2 = y_0, \qquad ac_3 = -\Omega x_0.$$

Solving the above equations, we obtain

$$c_1 = \frac{2\Omega^2 y_0}{a^2}, \qquad c_2 = \frac{(\gamma_y^2 + \Omega^2)y_0}{a^2}, \qquad c_3 = -\frac{\Omega x_0}{a}, \qquad c_4 = \frac{(\gamma_y^2 + \Omega^2)x_0}{a^2}. \tag{2.35}$$

Thus the solution (2.26), (2.27) is a combination of (2.33), (2.34) and (2.35). □

Similarly for $\gamma_x < |\Omega| = \gamma_y$, we have

Lemma 2.3. *If $\gamma_x < \gamma_y = |\Omega|$ in (2.4)–(2.6), the solutions $x(t)$ and $y(t)$ for the motion of the center are*

$$x(t) = \frac{x_0}{a^2}\left[2\Omega^2 + \left(\gamma_x^2 + \Omega^2\right)\cos(at)\right] + \frac{\Omega y_0}{a}\sin(at), \quad t \geqslant 0, \tag{2.36}$$

$$y(t) = \frac{y_0}{a^2}\left[\left(\gamma_x^2 + \Omega^2\right) + 2\Omega^2\cos(at)\right] + \frac{\Omega x_0}{a^2}\left[\left(\gamma_x^2 - \Omega^2\right)t - \frac{2(\gamma_x^2 + \Omega^2)}{a}\sin(at)\right], \tag{2.37}$$

where $a = \sqrt{\gamma_x^2 + 3\Omega^2}$. Again this implies that the center moves on an ellipse when $x_0 = 0$, and moves to infinity when $x_0 \neq 0$.

Proof. Follows the line of the analogous results in Lemma 2.2. □

Fig. 5 plots the time evolution of the center $\mathbf{x}(t)$ with $\Omega = \gamma_x = 1 < \gamma_y = 2$ for different $\mathbf{x}_0$. From it and our additional results, we can get: (i) When $|\Omega| = \gamma_x < \gamma_y$, if $y_0 \neq 0$, the trajectory of the center is a spiral coil going to infinity in x-direction (cf. Fig. 5(a)), while if $y_0 = 0$, the trajectory is an ellipse (cf. Fig. 5(b)). (ii) When $\gamma_x < \gamma_y = |\Omega|$, if $\mathbf{x}_0 \neq 0$, the trajectory is a spiral coil going to infinity in y-direction; if $x_0 = 0$, it is an ellipse.

If $\Omega \neq 0$, γ_x or γ_y, we denote $\delta_1 = (\gamma_x^2 + \gamma_y^2 + 2\Omega^2)/2$, $\delta_2 = \sqrt{\delta_1^2 - (\gamma_x^2 - \Omega^2)(\gamma_y^2 - \Omega^2)}$, $a = \sqrt{|\delta_1 - \delta_2|}$ and $b = \sqrt{\delta_1 + \delta_2}$. When $0 < |\Omega| < \gamma_x$ or $|\Omega| > \gamma_y$, we have $0 < \delta_2 < \delta_1$. Thus the four roots of the characteristic equation (2.13) are

$$\lambda_{1,2} = \pm i\sqrt{\delta_1 - \delta_2} = \pm ai, \qquad \lambda_{3,4} = \pm i\sqrt{\delta_1 + \delta_2} = \pm bi. \tag{2.38}$$

Following the procedure in the proof of Lemma 2.1, after a detailed computation, we get the solution of the ODE system (2.4)–(2.6) in this case:

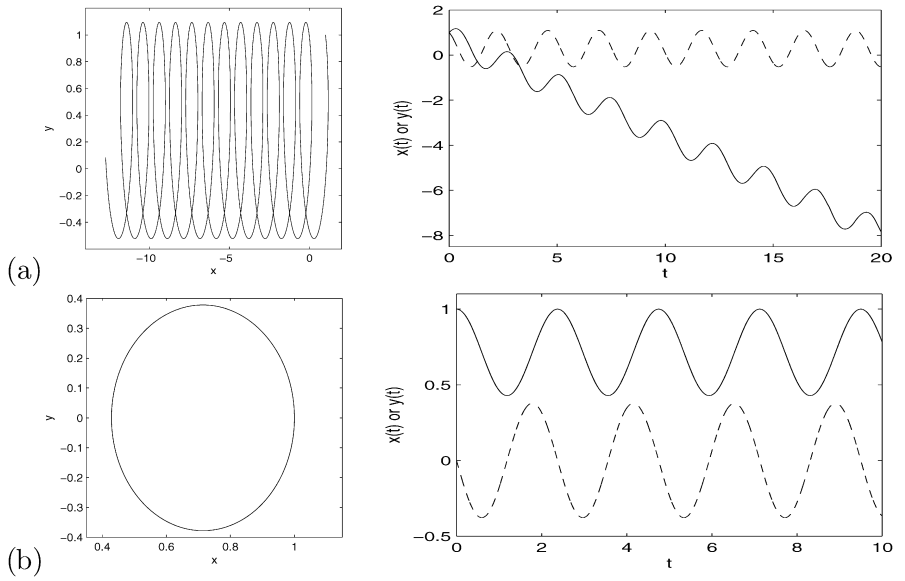

Fig. 5. Motion of the center $\mathbf{x}(t)$ in 2D for a rotating BEC. Left: trajectory $\mathbf{x}(t)$ for $t \in [0, 30]$; Right: time evolution of $x(t)$ (solid line) and $y(t)$ (dash line). (a) $\mathbf{x}_0 = (1, 1)^T$; (b) $\mathbf{x}_0 = (1, 0)^T$.

Lemma 2.4. *If $\gamma_x < \gamma_y$, and $0 < |\Omega| < \gamma_x$ or $|\Omega| > \gamma_y$, we have the solution $x(t)$ and $y(t)$ of the ODE system* (2.4)–(2.6) *as*

$$x(t) = c_1 \cos(at) + c_2 \sin(at) + c_3 \cos(bt) + c_4 \sin(bt), \tag{2.39}$$

$$y(t) = c_5 \cos(at) + c_6 \sin(at) + c_7 \cos(bt) + c_8 \sin(bt), \quad t \geqslant 0, \tag{2.40}$$

where

$$c_1 = \frac{(\gamma_x^2 + \Omega^2 - b^2)x_0}{a^2 - b^2}, \qquad c_2 = \frac{a\Omega(\gamma_x^2 - \Omega^2 + b^2)y_0}{(\gamma_x^2 - \Omega^2)(a^2 - b^2)},$$

$$c_3 = -\frac{(\gamma_x^2 + \Omega^2 - a^2)x_0}{a^2 - b^2}, \qquad c_4 = -\frac{b\Omega(\gamma_x^2 - \Omega^2 + a^2)y_0}{(\gamma_x^2 - \Omega^2)(a^2 - b^2)},$$

$$c_5 = -\frac{(\gamma_x^2 - \Omega^2 - a^2)(\gamma_x^2 - \Omega^2 + b^2)y_0}{2(\gamma_x^2 - \Omega^2)(a^2 - b^2)}, \qquad c_6 = \frac{(\gamma_x^2 - \Omega^2 - a^2)(\gamma_x^2 + \Omega^2 - b^2)x_0}{2a\Omega(a^2 - b^2)},$$

$$c_7 = \frac{(\gamma_x^2 - \Omega^2 + a^2)(\gamma_x^2 - \Omega^2 - b^2)y_0}{2(\gamma_x^2 - \Omega^2)(a^2 - b^2)}, \qquad c_8 = -\frac{(\gamma_x^2 - \Omega^2 - b^2)(\gamma_x^2 + \Omega^2 - a^2)x_0}{2b\Omega(a^2 - b^2)}.$$

This implies that the graph of the trajectory is a bounded set.

Similarly, when $\gamma_x < |\Omega| < \gamma_y$, we have $\delta_2 > \delta_1$, and the four roots of the characteristic equation (2.13) are

$$\lambda_{1,2} = \pm\sqrt{\delta_2 - \delta_1} = \pm a, \qquad \lambda_{3,4} = \pm i\sqrt{\delta_1 + \delta_2} = \pm bi. \tag{2.41}$$

Following the procedure in the proof of Lemma 2.1, after a detailed computation, we get the solution of the ODE system (2.4)–(2.6) in this case:

Lemma 2.5. *If $\gamma_x < |\Omega| < \gamma_y$, we have the solution $x(t)$ and $y(t)$ of the ODE system* (2.4)–(2.6) *as*

$$x(t) = d_1 e^{at} + d_2 e^{-at} + d_3 \cos(bt) + d_4 \sin(bt), \tag{2.42}$$

$$y(t) = d_5 e^{at} + d_6 e^{-at} + d_7 \cos(bt) + d_8 \sin(bt), \quad t \geqslant 0, \tag{2.43}$$

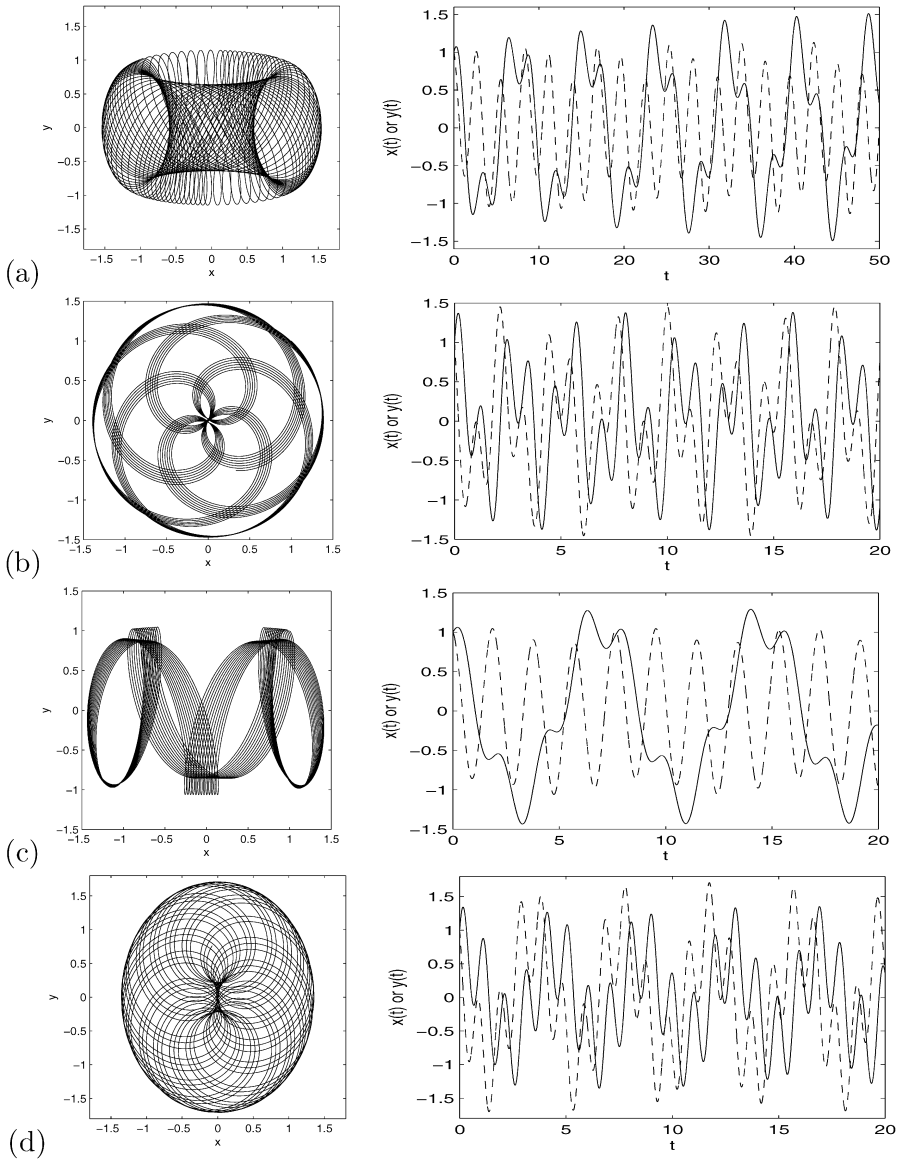

Fig. 6. Motion of the center $\mathbf{x}(t)$ in 2D for a rotating BEC. Left: trajectory $\mathbf{x}(t)$ for $t \in [0, 100]$; Right: time evolution of $x(t)$ (solid line) and $y(t)$ (dash line). (a) $\Omega = 1/2$, $\gamma_x = 1$, $\gamma_y = 2$; (b) $\Omega = 4$, $\gamma_x = 1$, $\gamma_y = 2$; (c) $\Omega = 1/2$, $\gamma_x = 1$, $\gamma_y = \pi$; (d) $\Omega = 4$, $\gamma_x = 1$, $\gamma_y = \pi$.

where

$$d_1 = \frac{1}{2}(c_1 - c_2), \qquad d_2 = -\frac{1}{2}(c_1 + c_2), \qquad d_3 = c_3, \qquad d_4 = c_4, \qquad d_7 = c_7, \qquad d_8 = c_8,$$
$$d_5 = \frac{(\gamma_x^2 - \Omega^2 + a^2)}{4a\Omega}(c_1 - c_2), \qquad d_6 = \frac{(\gamma_x^2 - \Omega^2 + a^2)}{4a\Omega}(c_1 + c_2),$$

with $c_1, \ldots, c_8$ *constants defined in Lemma* 2.4. *From the above solution, we can see that if* $c_1 = c_2$, *i.e.* $y_0 = \frac{(\gamma_x^2 - \Omega^2)(\gamma_x^2 + \Omega^2 - b^2)x_0}{a\Omega(\gamma_x^2 - \Omega^2 + b^2)}$, *the graph of the trajectory is a bounded set; otherwise, the center will move to the infinity exponentially fast and satisfies*

$$\lim_{t\to\infty} \frac{y(t)}{x(t)} = \frac{d_5}{d_1} = \frac{(\gamma_x^2 - \Omega^2 + a^2)}{2a\Omega}. \tag{2.44}$$

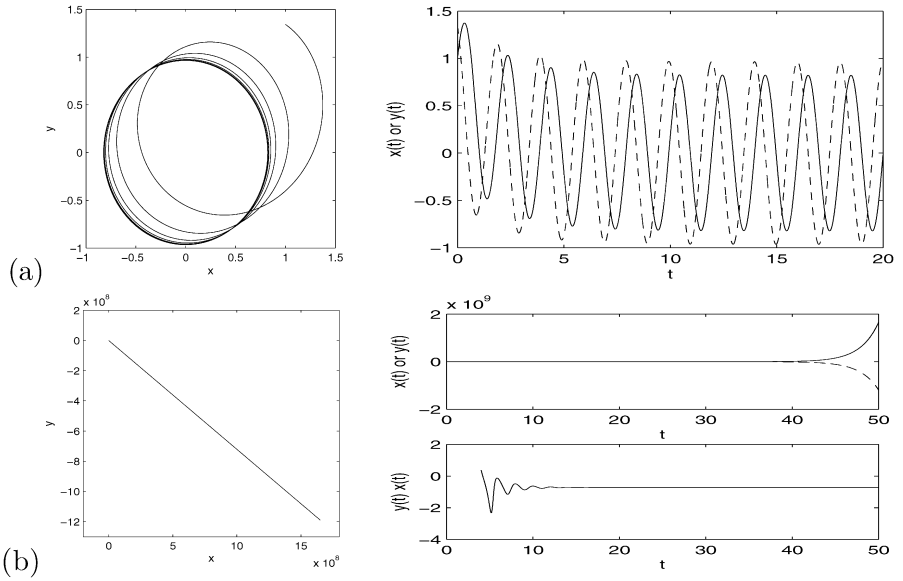

Fig. 7. Motion of the center $\mathbf{x}(t)$ in 2D for a rotating BEC with $1 = \gamma_x < \Omega = 1.5 < \gamma_y = 2$. Left: trajectory $\mathbf{x}(t)$ for $t \in [0, 50]$; Right: time evolution of $x(t)$ (solid line) and $y(t)$ (dash line). (a) $\mathbf{x}_0 = (1, 1.3424)^T$; (b) $\mathbf{x}_0 = (1, 1)^T$.

Fig. 6 plots the time evolution of the center $\mathbf{x}(t)$ with $\mathbf{x}_0 = (1, 1)^T$ for different $\gamma_x < \gamma_y$ and Ω which satisfy $|\Omega| < \gamma_x$ or $|\Omega| > \gamma_y$. Fig. 7 shows similar results with $1 = \gamma_x < |\Omega| = 1.5 < \gamma_y = 2$ for different $\mathbf{x}_0$. From Figs. 6 and 7, we can draw the following conclusions: (i) When $\gamma_x < \gamma_y$, and $0 < |\Omega| < \gamma_x$ or $|\Omega| > \gamma_y$, the center moves chaotically in a bounded domain (cf. Fig. 6). (ii) When $\gamma_x < |\Omega| < \gamma_y$, if $y_0 = \frac{(\gamma_x^2 - \Omega^2)(\gamma_x^2 + \Omega^2 - b^2)x_0}{a\Omega(\gamma_x^2 - \Omega^2 + b^2)}$, the center moves in a bounded domain (cf. Fig. 7(a)); otherwise it would move to the infinity exponentially fast, and after a short time, it almost moves along a straight line with slope $\frac{(\gamma_x^2 - \Omega^2 + a^2)}{2a\Omega}$ (cf. Fig. 7(b)).

3. Numerical method and results

Due to the trapping potential $V_d(\mathbf{x})$, the solution $\psi(\mathbf{x}, t)$ of the GPE (1.1) decays to zero exponentially fast when $|\mathbf{x}| \to \infty$. Thus in practical computation, we can truncate the problem (1.1), (1.2) into a bounded computational domain $\Omega_{\mathbf{x}}$ with the homogeneous Dirichlet boundary condition, where in 2D $\Omega_{\mathbf{x}} = [a, b] \times [c, d]$, and respectively in 3D $\Omega_{\mathbf{x}} = [a, b] \times [c, d] \times [e, f]$ with $|a|$, b, $|c|$, d, $|e|$ and f sufficiently large. For simplicity, here we present the numerical method for 2D case, and generalization to 3D is straightforward.

Choose a time step $\Delta t > 0$ and spatial mesh sizes $\Delta x = (b - a)/J$ and $\Delta y = (d - c)/K$ with J and K even integers. Denote the grid points as $x_j = a + j\Delta x$ and $y_k = c + k\Delta y$ with $0 \leqslant j \leqslant J$ and $0 \leqslant k \leqslant K$, and let $\psi_{j,k}^n$ be the approximation of $\psi(x_j, y_k, t_n)$. Then for $n = 1, 2, \ldots$, from time $t = t_{n-1} = (n - 1)\Delta t$ to $t = t_{n+1} = (n + 1)\Delta t$, we can discretize the GPE by the Fourier pseudospectral method in space and the leap-frog scheme in time, i.e. for $1 \leqslant j \leqslant J - 1$ and $1 \leqslant k \leqslant K - 1$,

$$i\frac{\psi_{j,k}^{n+1} - \psi_{j,k}^{n-1}}{2\Delta t} = -\frac{1}{2}\big(\nabla_h^2 \psi^n\big)\big|_{j,k} + V_2(x_j, y_k)\psi_{j,k}^n + \beta_2\big|\psi_{j,k}^n\big|^2\psi_{j,k}^n - \Omega\big(L_h\psi^n\big)\big|_{j,k}, \tag{3.1}$$

where ∇_h^2 and L_h, the pseudospectral differential operators approximating the operators ∇^2 and L_z respectively, are defined as

$$\big(\nabla_h^2\psi^n\big)\big|_{j,k} = -\sum_{p=-J/2}^{J/2-1}\sum_{q=-K/2}^{K/2-1}\big(\mu_p^2 + \lambda_q^2\big)\big(\widehat{\psi^n}\big)_{p,q}\, e^{i\mu_p(x_j - a)}\, e^{i\lambda_q(y_k - c)}, \tag{3.2}$$

$$\big(L_h\psi^n\big)\big|_{j,k} = x_j\big(D_y^h\psi^n\big)\big|_{j,k} - y_k\big(D_x^h\psi^n\big)\big|_{j,k}, \quad 0 \leqslant j \leqslant J,\ 0 \leqslant k \leqslant K, \tag{3.3}$$

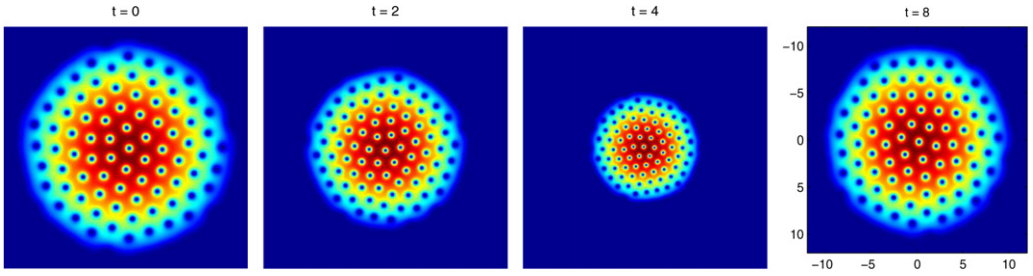

Fig. 8. Contour plots of the density $|\psi(\mathbf{x},t)|^2$ of the vortex lattices at different times.

$$\left(D_x^h\psi^n\right)\big|_{j,k} = \sum_{p=-J/2}^{J/2-1}\sum_{q=-K/2}^{K/2-1} \mu_p\left(\widehat{\psi^n}\right)_{p,q} e^{i\mu_p(x_j-a)}\, e^{i\lambda_q(y_k-c)}, \tag{3.4}$$

$$\left(D_y^h\psi^n\right)\big|_{j,k} = \sum_{p=-J/2}^{J/2-1}\sum_{q=-K/2}^{K/2-1} \lambda_q\left(\widehat{\psi^n}\right)_{p,q} e^{i\mu_p(x_j-a)}\, e^{i\lambda_q(y_k-c)}, \tag{3.5}$$

with

$$\mu_p = \frac{2p\pi}{b-a}, \quad p = -\frac{J}{2},\ldots,\frac{J}{2}-1; \qquad \lambda_q = \frac{2q\pi}{d-c}, \quad q = -\frac{K}{2},\ldots,\frac{K}{2}-1,$$

$$\left(\widehat{\psi^n}\right)_{p,q} = \frac{1}{JK}\sum_{j=0}^{J-1}\sum_{k=0}^{K-1} \psi_{j,k}^n\, e^{-i\mu_p(x_j-a)}\, e^{-i\lambda_q(y_k-c)}.$$

To compute $\psi_{j,k}^1$, we apply the modified trapezoidal rule on the interval $[0,t_1]$, i.e.

$$\begin{aligned}
i\frac{\psi_{j,k}^{(1)}-\psi_{j,k}^0}{\Delta t} &= -\frac{1}{2}\left(\nabla_h^2\psi^0\right)\big|_{j,k} + V_2(x_j,y_k)\psi_{j,k}^0 + \beta_2\left|\psi_{j,k}^0\right|^2\psi_{j,k}^0 - \Omega\left(L_h\psi^0\right)\big|_{j,k},\\
i\frac{\psi_{j,k}^{(2)}-\psi_{j,k}^{(1)}}{\Delta t} &= -\frac{1}{2}\left(\nabla_h^2\psi^{(1)}\right)|_{j,k} + V_2(x_j,y_k)\psi_{j,k}^{(1)} + \beta_2|\psi_{j,k}^{(1)}|^2\psi_{j,k}^{(1)} - \Omega\left(L_h\psi^{(1)}\right)\big|_{j,k},\\
\psi_{j,k}^1 &= \frac{1}{2}\left(\psi_{j,k}^{(1)}+\psi_{j,k}^{(2)}\right), \quad 1\leqslant j\leqslant J-1,\ 1\leqslant k\leqslant K-1.
\end{aligned} \tag{3.6}$$

The leap-frog Fourier pseudospectral (LFFP) discretization (3.1)–(3.5) is explicit and time reversible. It is of spectral accuracy in space and second-order accuracy in time. The total memory requirement is $O(JK)$ and the total computational cost per time step is $O(JK\ln(JK))$. Following the standard von Neumann analysis, the stability condition is

$$\Delta t < \frac{2(\Delta x)^2}{\pi^2[1+(\frac{\Delta x}{\Delta y})^2] + 2(\Delta x)^2\max_{\mathbf{x}\in\Omega_{\mathbf{x}}}[\pi|\Omega|(\frac{|x|}{\Delta x}+\frac{|y|}{\Delta y}) + V_2(\mathbf{x}) + \beta_2|\psi(\mathbf{x},t)|^2]}.$$

To show the effectiveness of the LFFP method, we apply it to study the dynamics of a quantized vortex lattice with 81 vortices in rotating BEC. The parameters are chosen as $d=2$, $\beta_2=2000$, $\Omega=0.9$, and the initial data in (1.2) is the ground state [6,3,1] computed numerically with the same parameters and $\gamma_x=\gamma_y=1$. Then at $t=0$, we change the trap frequency by setting $\gamma_x=\gamma_y=1.5$. Fig. 8 shows contour plots of the density $|\psi(\mathbf{x},t)|^2$ at different times.

From Fig. 8, we can see that initially there are 81 quantized vortices in the ground state. During the time evolution, the lattice shrinks or expands due to the changing of the trapping frequencies. This clearly demonstrates the high resolution of the LFFP method.

4. Conclusion

We have solved analytically the second-order ordinary differential system which governs the motion of the center of mass in the dynamics of a stationary state with its center shifted. Based on the analytical solutions, we classified

different motion patterns of the center and provided some mathematical justifications for the observations in [3] for the motion. The results from the ODE system were confirmed by directly simulating the GPE with an isotropic potential. We also presented a leap-frog Fourier pseudospectral (LFFP) method for efficient and accurate simulations of the GPE in a rotational frame. Our numerical results demonstrated the spectral resolution in space of the LFFP method.

Acknowledgement

The authors acknowledge support by the National University of Singapore grant No. R-151-000-035-112. W.B. also thanks hospitality during his extended visit at Department of Mathematics, Capital Normal University where part of the work was carried out.

References

[1] A. Aftalion, Q. Du, Vortices in a rotating Bose–Einstein condensate: Critical angular velocities and energy diagrams in the Thomas–Fermi regime, Phys. Rev. A 64 (2001) 063603–063613.
[2] M.H. Anderson, J.R. Ensher, M.R. Matthewa, C.E. Wieman, E.A. Cornell, Observation of Bose–Einstein condensation in a dilute atomic vapor, Science 269 (1995) 198–201.
[3] W. Bao, Q. Du, Y. Zhang, Dynamics of rotating Bose–Einstein condensates and their efficient and accurate numerical computation, SIAM J. Appl. Math. 66 (2006) 758–786.
[4] W. Bao, D. Jaksch, P.A. Markowich, Numerical solution of the Gross–Pitaevskii equation for Bose–Einstein condensation, J. Comput. Phys. 187 (2003) 318–342.
[5] W. Bao, J. Shen, A fourth-order time-splitting Laguerre–Hermite pseudo-spectral method for Bose–Einstein condensates, SIAM J. Sci. Comput. 26 (2005) 2010–2028.
[6] W. Bao, H. Wang, P.A. Markowich, Ground, symmetric and central vortex states in rotating Bose–Einstein condensates, Comm. Math. Sci. 3 (2005) 57–88.
[7] W. Bao, Y. Zhang, Dynamics of the ground state and central vortex states in Bose–Einstein condensation, Math. Models Methods Appl. Sci. 15 (2005) 1863–1896.
[8] M.M. Cerimele, F. Pistella, S. Succi, Particle-inspired scheme for the Gross–Pitaevskii equation: An application to Bose–Einstein condensation, Comput. Phys. Comm. 129 (2000) 82–90.
[9] J.J. Garcia-Ripoll, V.M. Perez-Garcia, V. Vekslerchik, Construction of exact solutions by spatial translations in inhomogeneous nonlinear Schrodinger equations, Phys. Rev. E 64 (2001) 056602–056607.
[10] K.W. Madison, F. Chevy, V. Bretin, J. Dalibard, Stationary states of a rotating Bose–Einstein condensate: Routes to vortex nucleation, Phys. Rev. Lett. 86 (2001) 4443–4446.
[11] M.R. Matthews, B.P. Anderson, P.C. Haljan, D.S. Hall, C.E. Wiemann, E.A. Cornell, Vortices in a Bose–Einstein condensates, Phys. Rev. Lett. 83 (1999) 2498–2501.
[12] P. Muruganandam, S.K. Adhikari, Bose–Einstein condensation dynamics in three dimensions by pseudospectral and finite-difference methods, J. Phys. B: At. Mol. Opt. Phys. 36 (2003) 2501–2513.